Chapter 5

Graphene mechanics studied by biaxial compression: The effect of sp^3 and vacancy defects

This work studies the mechanics of graphene floating on the surface of water, subject to biaxial compression in a Langmuir-Blodgett (LB) trough. The platform uniquely allows to characterize graphene samples with centimeter-scale lengths, four orders of magnitude larger than commonly probed microscale graphene samples. The full stress-strain diagram of graphene was plotted to identify elastic and plastic deformation regions. The Young's modulus respects a predicted scaling law and falls two orders of magnitude below that for flat graphene. In contrast, the rigidity of graphene against out-of-plane deformations (flexural rigidity) strongly improves in our large samples. These results demonstrate that graphene – in its very natural form – lacks any intrinsic elastic parameters. Functionalization of the graphene lattice affects the mechanics of graphene; particularly the effects of the sp^3 hybridization and crystalline voids are explored. This work elucidates yet-unexplored science of graphene and establish novel applications for this material in mechanical systems.

Part of this chapter was prepared as an article: Hadi Arjmandi-Tash, Hessam Sokooti, Khosrow Shakouri, Lin Jiang, Alexander Kloosterman, Marius Staring, Lia M.C. Lima, and Grégory F. Schneider, manuscript in preparation.

5.1 Introduction

Picturing graphene as a strictly two-dimensional sheet is unrealistic; though dubbed as two-dimensional, the surface of such materials indeed exhibit transverse out-of-plane undulations (the bending modes) with limited amplitudes in addition to the expected in-plane undulations (stretching modes). Both the in-plane and transverse undulations contribute to the total elastic energy. Harmonic approximation provides a fast solution for this energy considering that the dual modes are decoupled. In this approximation, the average amplitude of the transverse undulations scales with L^2 (L: size of the sample) and approaches infinity for large samples.[1] This result was interpreted as the tendency for crumpling which questioned the existence of graphene for several decades.[2]

A more realistic solution, however, was achieved considering that the bending and stretching modes are coupled and mutually affect each other (anharmonic approximation). The transverse displacements are now considerably weaker and scale with $L^{1-\eta/2}$ ($\eta = 0.8$), though still larger than the interatomic distances. Indeed the approximation predicts an intrinsic tendency for small amplitude transverse undulations which eventually and thermodynamically stabilizes the material. The undulations are still size-dependent which activate size-dependent elastic properties. Particularly atomistic Monte Carlo (MC) simulations demonstrates that the out-of-plane undulations in anharmonic approximation renormalize the in-plane stiffness of graphene as $\sim L^{-0.325}$ (L: size of the sample).[3] The effect, however, cannot be experimentally measured using existing standard platforms (e.g. nano-indentation experiments[4] and graphene nano-resonators[5] where graphene is subject to tensile loadings. Indeed the tensile strain suppresses the anharmonicity.[6] The lack of a suitable experimental approach, on the other hand, has limited the knowledge about the performance of graphene under compression.

In fact compressing free-standing graphene is impractical as graphene collapses. Once supported on a rigid substrate, however, the out-of-plane deformations inherited from the corrugations on the surface of the substrate and graphene/substrate interactions affect the experiment.[7] More importantly, the mechanics of the substrate is involved in the measurements[8] and decoupling the contributions of graphene and the substrate is complex. Such experiments may lack accuracy also as a result of the lateral slippage of graphene during the experiments.[9]

Water offers numerous advantages to conduct graphene compression experiments, hardly available with rigid substrates: i) The surface of water is strictly planar and serves as an appropriate substrate for the two-dimensional graphene. ii) The

adhesion energy between hydrophobic graphene and water is lower than graphene on typical substrates[10] (45 times lower than graphene on silicon), which guarantees a negligible graphene/substrate interaction. In addition, iii) graphene can smoothly slide on the surface of water (no dry friction) which allows free deformation upon compressive buckling. It is important that iv) ultra-pure water is easily accessible; the uniform and simple chemistry of the water substrate is not a source of irreproducibility, demonstrating that it is now possible to probe still unexplored properties of graphene.

5.2 Results

5.2.1 Compression of graphene floating on water

The study was performed on a LB trough, capable of applying a precisely controlled two dimensional pressure on graphene under test while freely floating at air/water interface.[11] A piece of ~1 × 1 cm^2 crack-free graphene,[12] chemically grown on a copper foil,[13] was placed on the surface of an ammonium persulfate solution (0.5 M) on the trough and surrounded with Dipalmitoylphosphatidylcholine (DPPC) (see Figure AIV. 1 and Appendix IV. 2). Once the copper foil etches away, graphene was freely floating at the air/liquid interface. Unlike the compression of graphene embedded in polymeric materials where the placement of graphene or curing the supporting polymer deposit a residual strain (which adds complexity to the analysis),[9a] graphene in our experiments can relax to release any strain (e.g. due to the growth) before initiating the measurements.

Moving two slightly-wetted solid barriers – initially positioned at opposite sides of the trough – forward (closer to each other) lowers the accessible area which eventually applies a two-dimensional surface pressure p (referred to as stress) to graphene (Figure 5.1a). The role of the lipid molecules is to form a stable, two-dimensional and dynamic self-assembled layer at the air/liquid interface in contact with graphene ensuring a strictly lateral compression (no perpendicular component) of graphene. The two-dimensional strain ($\varepsilon_{||} = (A_0 - A)/A_0$, A_0: initial area of graphene, A: area of graphene at the time of the measurement) of the graphene was estimated by processing high resolution images taken by a camera focusing on graphene (see Methods in AIV).

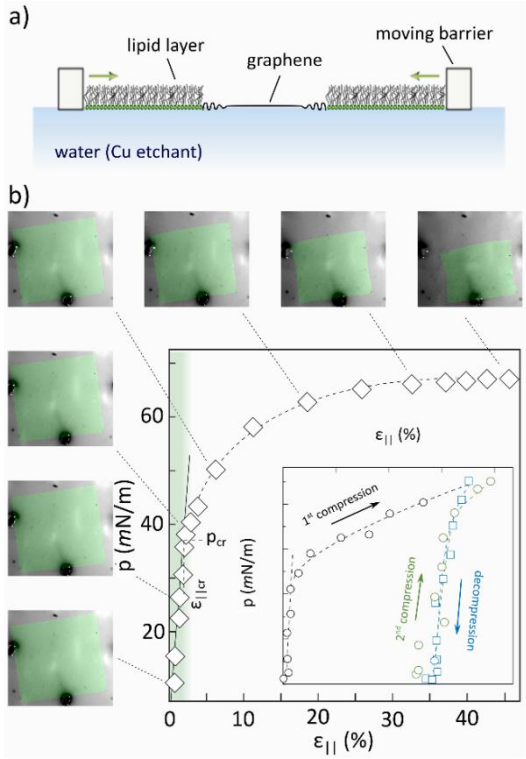

Figure 5.1 Floating graphene subject to 2D compression. a) Schematic representation of the experimental set-up: graphene floating on the surface of a copper etchant (0.5 M ammonium persulfate) is subject to a compressive stress applied by surrounding lipids and moving barriers. b) Stress-strain relation of a floating graphene piece (~1 × 1 cm²): The green shaded area in the main plot corresponds to the elastic deformation region with the solid line as the linear fit. Few snapshots of the graphene (colored in green) at different compression stages are presented at the left and top margins, featuring progressive deformations upon compression. Inset panel corresponds to the subsequent compression (black)/decompression (blue)/compression (green) of a separate graphene sheet. The horizontal displacement between the first and second compression strokes corresponds to the permanent plastic deformation. The barrier displacement rate was limited to 1 mm/min in these experiments.

Figure 5.1b shows the stress-strain curve of a selected graphene sample. Similar to conventional materials, graphene exhibits an elastic deformation (linear stress-strain relation) up to a certain level (critical stress p_{cr}); Then plastic deformation, characterized by the buckling of graphene, starts. Unlike elastic deformation which is reversible, plastic deformation is permanent: removing the external pressure, does not return graphene to its original shape (inset Figure 5.1b). Bulk modulus (k) in biaxial loading measures the resistance of the material against elastic deformation: $p = k\varepsilon_{||}$ and scales with the two dimensional Young's modulus (E_{2D}) as: $k =$

$E_{2D}/2(1-\vartheta)$ where $\vartheta = 0.25$ is the Poisson's ratio of the graphene estimated for large samples.[3]

5.2.2 The introduction of lattice defects

Sp^3 hybridization of carbon orbitals (as a result of reaction with various chemical components) and vacancy defects (generated by shooting-out carbon atoms in momentum transfer processes) are the two major defect types commonly observed in graphene lattice. The mechanics of graphene in the presence of such defects was characterized. Hydrogenation of graphene and argon bombardment of the lattice in a plasma chamber respectively achieved sp^3 hybridization and vacancy defects. Manipulation of the lattice affects the mechanics of graphene. Inclusion of the crystalline defects upon exposing the graphene samples to argon and hydrogen plasmas modify the mechanics of graphene. The defect density n_D can be estimated using the relative intensities of the Raman D and G peaks[14]:

$$n_D\ [cm^{-2}] = (7.3 \pm 2.2) \times 10^9 E_L^4 (I_D/I_G) \quad (1)$$

In this relation $E_L = 2.33$ eV is the excitation energy. Figure 5.2 shows the Raman spectra and defect density characterization for samples treated by argon (a-b) and hydrogen plasma (c-d). Note that the intercept of the polynomial fitting of the time dependent defect density gives $n_0 = 9 \times 10^{10}$ cm^{-2} for untreated graphene samples. Energetic Ar^+ ions in plasma bombardment of graphene are capable to effectively knock-out carbon atoms from the lattice and generate vacancy defects of atomic sizes.[15] In contrast, hydrogen radicals are chemically active and form covalent bonds to carbon atoms, altering their hybridization state from sp^2 to sp^3.[16]

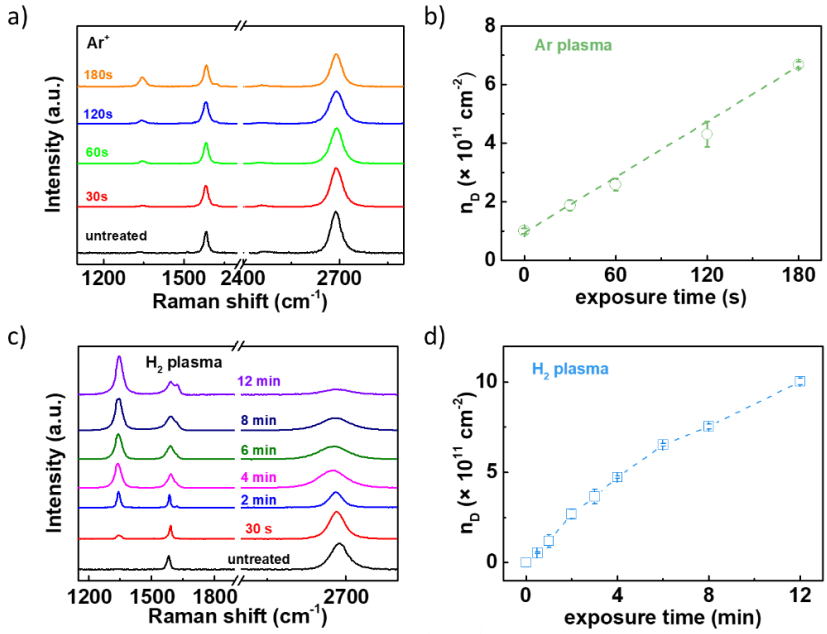

Figure 5.2 Raman characterization and mechanics of functionalized graphene samples. a) Typical Raman spectra recorded on graphene samples exposed to Ar plasma for different durations. b) Density of the vacancy defects (n_D) calculated for different samples in (a). c) Typical Raman spectra recorded on graphene samples exposed to H_2 plasma for different durations. d) Density of the sp^3 hybridization defects calculated for different samples in (c). All the Raman spectra were recorded on graphene/silica wafers, using an excitation source of λ = 532 nm.

5.2.3 Elastic properties of compressed graphene

It is commonly said that pristine graphene, possessing strong bonds between the carbon atoms, is one of the most stiff materials (few hundred times stiffer than steel[4a]) featuring a Young's modulus of $E_{2D}^{flat} \sim 336\ {}^{N}/_{m}$.[17] Such a statement has to be used with care as its validity is limited to graphene samples that are free from out-of-plane perturbations (flat graphene). Indeed tensile loading of the samples, as the standard procedure to probe the stiffness of graphene so far,[4-5] inevitably flattens graphene and suppress anharmonicity.[6, 18] Our approach is the only existing method so far which measures the stiffness of graphene while the natural perturbations remain untouched. The median Young's moduli of our twenty monolayer graphene samples approaches $\bar{E}_{2D}$ = 2.6 N m^{-1} (k = 1.7 N m^{-1}) (Figure 5.3a). Remarkably, this value is two orders of magnitude smaller than E_{2D}^{flat} but can be well-explained in the framework of the scaling effect in the presence of the anharmonicity (Figure 5.3b and Appendix IV. 3): Indeed for large samples, the lower energy costs of out of plane fluctuations ($\propto q^2$, q: the wave vector) compared to in-plane ones ($\propto q$) favors the

long wavelength out-of-plane fluctuations and increases the contribution of the anharmonic energy correction terms in total elastic energy. The size dependency of the energy terms causes a size dependent stiffness which falls in large samples. Interestingly the stiffness of our centimeter-scale samples falls on the extrapolation and respects the same scaling law of the samples of few (tens of) nanometer size (~ six orders of magnitude smaller in size, ~twelve orders of magnitude larger in area, more relevant for 2D compression) and validates the accuracy of those modelling.

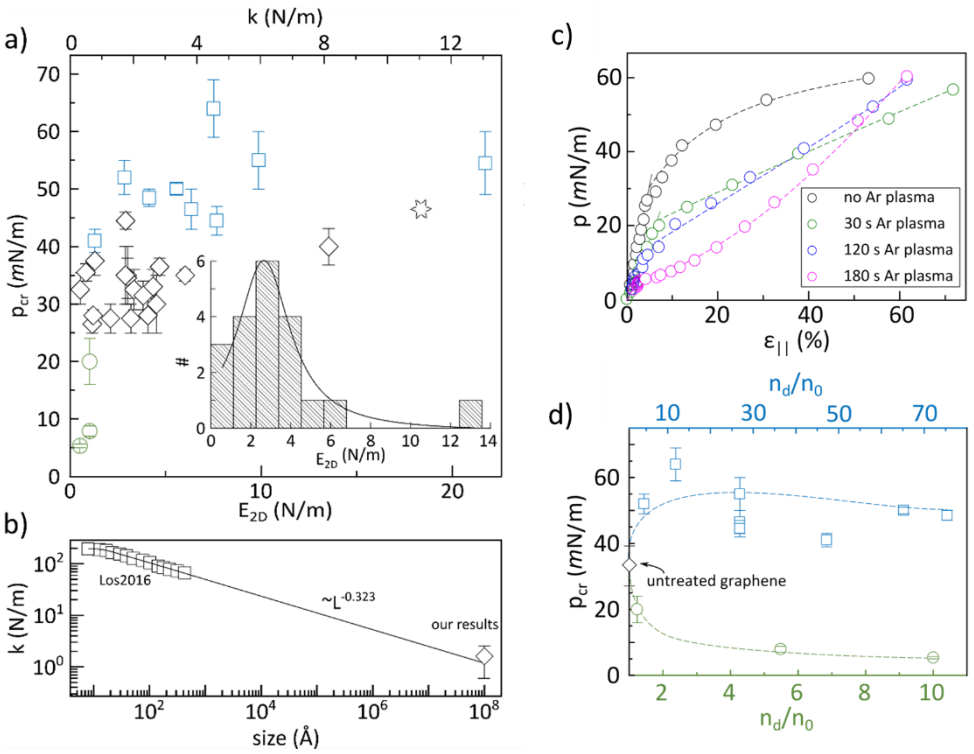

Figure 5.3 Elastic properties of graphene subject to 2D compression. a) Correlation of the yield strength and in-plane stiffness of untreated (monolayer: black diamonds, bilayer: black star), hydrogenated (blue squares), Ar^+ bombarded (green circles) graphene. The inset displays the distribution of the E_{2D} of untreated monolayer graphene samples, centered at 2.6 N m^{-1} with the FWHM of 3.2 N m^{-1} estimated by Lorentzian fitting (solid line). b) Superimposition our experimentally measured bulk moduli (untreated graphene) with the simulation results of nanoscale samples, by Los et. al.[3]: the solid line corresponds to the scaling law reported by the same group (Appendix IV. 3). c) Stress-strain plots of graphene samples subject to Ar ion bombardment of different durations. d) Critical pressure of hydrogenated and Ar ion bombarded graphene samples: the density of the defects (n_D) achieved by the Raman spectroscopy is normalized by the defect density of untreated graphene (n_0~ 9×10^9 cm^{-2}). The p_{cr} of untreated graphene is the median of all the measured samples detailed in Figure 1 of the main text. All the dashed lines are guides to the eyes.

Further characterization of the mechanics of graphene in the presence of such defects was conducted. Figure 5.3c details the stress-strain plots of graphene samples subject to Ar^+ bombardments of up to 180 s. Reduction of the p_{cr} at the cross-over between linear (elastic) and non-linear (plastic) deformations upon increasing the vacancy density is visible directly in the plots. Even after 180 s of plasma treatment, the relative concentration of the vacancies ($\sim 6 \times 10^{10}$ cm^{-2}) to the concentration of the carbon atoms in graphene lattice (3.82×10^{15} cm^{-2}) is negligible; hence the treatment is not expected to (and does not) affect the rigidity as it originates from the degree of order and the strength of the bonds between the atoms.[9a] In contrast, hydrogenation of graphene increases the p_{cr} (Figure 5.3d). Such an effect is attributed to the increased interaction between hydrogenated graphene lattice and water substrate (e.g. hydrogen bonds) which improves the in-plane Young's modulus upon partial screening of long wavelength flexural modes. It seems increasing the dose of the sp^3 defects ultimately (and gradually) tends to weaken the lattice.[19]

The inclusion of sp^3 defects (achieved by hydrogenation of the graphene lattice) considerably improves p_{cr}. Non-covalent graphene/substrate interaction has been observed to delay buckling by preventing the delamination of graphene from polymeric substrates.[7a, 9a] In a similar scenario, one could attribute the increase of p_{cr} to the apparition of hydrogen bonds between hydrogenated graphene and water in our system. In Appendix IV. 4 and 5, however, it is theoretically illustrated that water conforms graphene during the buckling and no delamination is involved. In fact, the increment in p_{cr} in hydrogenated graphene is a result of the improved Young's modulus, discussed below.

5.2.4 Correlation of strain and stiffness in graphene

Figure 5.4a shows the $\varepsilon_{|cr}\left(\approx \varepsilon_{||cr}/2\right)$ of different samples as a function of the stiffness. Untreated and hydrogenated samples respect the classical Eulerian picture of buckling[7a] and exhibit $\varepsilon_{|cr} \propto 1/E_{2D}$ behaviour. This trend is not observable with the Ar^+ bombarded samples. Notably, the hydrogenation of graphene improves the Young's modulus by $\beta = 1.5$ times, matching with the improvement in p_{cr} discussed in Figure 5.3a. In the framework of the anharmonic coupling the stretching and flexural modes in 2D materials and similar to an earlier observation,[4e] the improvement is attributed to the partial screening and eventual localization of the long wavelength flexural modes by sp^3 defects in hydrogenated graphene (Figure 5.4b). Particularly the improvement factor β is reasonably close to $(n_D/n_0)^{\eta/2}$ ($\eta = 0.36$) predicting 1.3 to 2.3 times improvement in Young's modulus.[4e] Our molecular dynamics simulations also confirms that the flexural modes are affected by hydrogenated sites,

leading to a 1.35 times improvement in Young's modulus, matching well with the experimental measurement (Figure AIV. 2b and c).

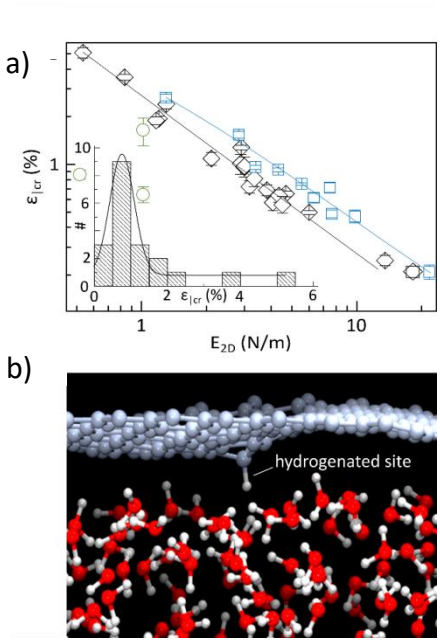

Figure 5.4 Correlation of the strain and stiffness in graphene. a) Correlation of the critical one-dimensional strain $\varepsilon_{|cr}$ $(\approx \varepsilon_{||cr}/2)$ and in-plane stiffness of untreated (monolayer: black diamonds, bilayer: black star), hydrogenated (blue squares), Ar^+ bombarded (green circles) graphene; the solid lines correspond to the best fittings with $\varepsilon_{|cr} = \frac{\alpha}{(E_{2D}/\beta)}$ revealing α = 0.027 N m^{-1} and β = 1 for untreated and α = 0.027 N m^{-1} and β = 1.4 for hydrogenated graphene. Inset shows the distribution of the $\varepsilon_{|cr}$ of untreated monolayer graphene, centred at 0.8%. b) Molecular dynamics simulation of hydrogenated graphene on the surface of water: interaction between the hydrogenated site and water molecules locally stabilizes the corresponding carbon atom. The snapshot corresponds to $\varepsilon < \varepsilon_{cr}$ region.

In the classical Eulerian picture of buckling, the coefficient α (see the fitting in Figure 5.4a) depends on the flexural rigidity *D* of the specimen. In Appendix IV. 6 and by analyzing the buckling patterns, *D* is estimated to be in the order of 10^{-12} N m (10^6 eV). The value for our centimeter-scale samples is at least three orders of magnitude larger than the previous report for micro-sized graphene samples[20] which itself is three to four orders of magnitude larger than for flat graphene. The trend agrees with the predicted scaling properties of flexible membranes.[21] Our observations of scaling both the Young's modulus and flexural rigidity demonstrates that graphene, in its natural form, lacks any intrinsic elastic coefficients.

Inset in Figure 5.4a plots the distribution of the critical strain of untreated graphene samples. Interestingly, the median critical strain ($\overline{\varepsilon}_{|cr} = 0.8\%$) in our centimetre-scale samples ($L/t \sim 10^8$) approaches that of narrow (micro-sized) graphene samples sandwiched in between polymeric supports;[7a] exhibiting such a large strain before buckling is attributed to the strictly 2D surface of water which excludes any substrate-induced out-of-plane deformations as buckling promoters.

5.3 Conclusion

Graphene floating on water remains in its natural form and now unlocked a versatile and easily accessible platform to study the mechanics of graphene, disclosing astonishing size-dependent in-plane and flexural rigidities. Particularly the Young's modulus of centimeter-scale graphene falls two-orders of magnitude below that in micrometer sized sheets, commonly measured earlier; The finding correct the regard to graphene as the strongest material ever measured. Chemical alteration of the graphene lattice remarkably affects the mechanics of the sheet. Particularly the inclusion of vacancy defects leads to a catastrophic failure in-which a negligible surface pressure causes graphene to collapse. Hydrogenation, however, locally stabilizes graphene on water leading to an improved in-plane stiffness. Compressing graphene floating on water, per se, provides new horizons both in science and application of graphene: piezoelectricity, surface chemistry, mechanics, material science, sensors, to name a few.

5.4 References

[1] A. Fasolino, J. H. Los, M. I. Katsnelson, *Nat. Mater.* **2007**, 6, 858.

[2] A. K. Geim, K. S. Novoselov, *Nat. Mater.* **2007**, 6, 183.

[3] J. H. Los, A. Fasolino, M. I. Katsnelson, *Phys. Rev. Lett.* **2016**, 116, 015901.

[4] a) C. Lee, X. Wei, J. W. Kysar, J. Hone, *Science* **2008**, 321, 385; b) G.-H. Lee, R. C. Cooper, S. J. An, S. Lee, A. van der Zande, N. Petrone, A. G. Hammerberg, C. Lee, B. Crawford, W. Oliver, J. W. Kysar, J. Hone, *Science* **2013**, 340, 1073; c) A. Zandiatashbar, G.-H. Lee, S. J. An, S. Lee, N. Mathew, M. Terrones, T. Hayashi, C. R. Picu, J. Hone, N. Koratkar, *Nat. Commun.* **2014**, 5, 3186; d) G. López-Polín, J. Gómez-Herrero, C. Gómez-Navarro, *Nano Lett.* **2015**, 15, 2050; e) G. López-Polín, C. Gómez-Navarro, V. Parente, F. Guinea, Mikhail I. Katsnelson, F. Pérez-Murano, J. Gómez-Herrero, *Nat. Phys.* **2014**, 11, 26.

[5] a) C. Chen, S. Rosenblatt, K. I. Bolotin, W. Kalb, P. Kim, I. Kymissis, H. L. Stormer, T. F. Heinz, J. Hone, *Nat. Nanotechnol.* **2009**, 4, 861; b) V. Singh, S. Sengupta, H. S. Solanki, R. Dhall, A. Allain, S. Dhara, P. Pant, M. M. Deshmukh, *Nanotechnology* **2010**, 21, 165204; c) A. M. v. d. Zande, R. A. Barton, J. S. Alden, C. S. Ruiz-Vargas, W. S. Whitney, P. H. Q. Pham, J. Park, J. M. Parpia, H. G. Craighead, P. L. McEuen, *Nano Lett.* **2010**, 10, 4869.

[6] R. Roldán, A. Fasolino, K. V. Zakharchenko, M. I. Katsnelson, *Phys. Rev. B* **2011**, 83, 174104.

[7] a) O. Frank, G. Tsoukleri, J. Parthenios, K. Papagelis, I. Riaz, R. Jalil, K. S. Novoselov, C. Galiotis, *ACS Nano* **2010**, 4, 3131; b) Z. H. Aitken, R. Huang, *J. Appl. Phys.* **2010**, 107, 123531.

[8] H. Conley, N. V. Lavrik, D. Prasai, K. I. Bolotin, *Nano Lett.* **2011**, 11, 4748.

[9] a) G. Tsoukleri, J. Parthenios, K. Papagelis, R. Jalil, A. C. Ferrari, A. K. Geim, K. S. Novoselov, C. Galiotis, *Small* **2009**, 5, 2397; b) T. Jiang, R. Huang, Y. Zhu, *Adv. Funct. Mater.* **2014**, 24, 396.

[10] J. Driskill, D. Vanzo, D. Bratko, A. Luzar, *J. Chem. Phys.* **2014**, 141, 18C517.

[11] P. Cicuta, D. Vella, *Phys. Rev. Lett.* **2009**, 102, 138302.

[12] H. Arjmandi-Tash, L. Jiang, G. F. Schneider, *Carbon* **2017**, 118, 556.

[13] H. Arjmandi-Tash, N. Lebedev, P. M. G. van Deursen, J. Aarts, G. F. Schneider, *Carbon* **2017**, 118, 438.

[14] L. G. Cançado, A. Jorio, E. M. Ferreira, F. Stavale, C. Achete, R. Capaz, M. Moutinho, A. Lombardo, T. Kulmala, A. C. Ferrari, *Nano Lett.* **2011**, 11, 3190.

[15] A. Eckmann, A. Felten, A. Mishchenko, L. Britnell, R. Krupke, K. S. Novoselov, C. Casiraghi, *Nano Lett.* **2012**, 12, 3925.

[16] J.-H. Zhong, J. Zhang, X. Jin, J.-Y. Liu, Q. Li, M.-H. Li, W. Cai, D.-Y. Wu, D. Zhan, B. Ren, *J. Am. Chem. Soc.* **2014**, 136, 16609.

[17] a) L. Pocivavsek, R. Dellsy, A. Kern, S. Johnson, B. Lin, K. Y. C. Lee, E. Cerda, *Science* **2008**, 320, 912; b) Y. Li, D. Datta, Z. Li, *Carbon* **2015**, 90, 234; c) M. M. Shokrieh, R. Rafiee, *Mater. Des.* **2010**, 31, 790; d) R. J. Young, I. A. Kinloch, L. Gong, K. S. Novoselov, *Compos. Sci. Technol.* **2012**, 72, 1459.

[18] J. H. Los, A. Fasolino, M. I. Katsnelson, *NPJ 2D Mater. Appl.* **2017**, 1, 9.

[19] G. López-Polín, C. Gómez-Navarro, V. Parente, F. Guinea, M. I. Katsnelson, F. Perez-Murano, J. Gómez-Herrero, *Nat. Phys.* **2015**, 11, 26.

[20] M. K. Blees, A. W. Barnard, P. A. Rose, S. P. Roberts, K. L. McGill, P. Y. Huang, A. R. Ruyack, J. W. Kevek, B. Kobrin, D. A. Muller, P. L. McEuen, *Nature* **2015**, 524, 204.

[21] J. H. Los, M. I. Katsnelson, O. V. Yazyev, K. V. Zakharchenko, A. Fasolino, *Phys. Rev. B* **2009**, 80, 121405.